ACS OMEGA

Article

Cite This: ACS Omega 2017, 2, 7576-7583

http://pubs.acs.org/journal/acsodf

Dual Probe Sensors Using Atomically Precise Noble Metal Clusters

Vidhya Subramanian,[†,‡] Sanjoy Jena,[§] Debasmita Ghosh,[†] Madhuri Jash,[†] Ananya Baksi,[†] Debdutta Ray,[§] and Thalappil Pradeep*[,†]

[†]DST Unit of Nanoscience (DSTUNS) and Thematic Unit of Excellence (TUE), Department of Chemistry, [‡]Department of Biotechnology, and [§]Department of Electrical Engineering, Indian Institute of Technology Madras, Chennai 600036, India

Supporting Information

ABSTRACT: This article adds a new direction to the functional capability of protein-protected atomically precise gold clusters as sensors. Counting on the extensively researched intense luminescence of these clusters and considering the electron donating nature of select amino acids, we introduce a dual probe sensor capable of sensing changes in luminescence and conductivity, utilizing bovine serum albumin-protected atomically precise gold clusters hosted on nanofibers. To this end, we have also developed a hybrid nanofiber with a conducting core with a porous dielectric shell. We show that clusters in combination with nanofibers offer a highly selective and sensitive platform for the detection of trace quantities of trinitrotoluene, both in solution and in the vapor phase. In the solution phase, trinitrotoluene (TNT) can be detected down to 1 ppt at room temperature, whereas in vapor phase, 4.8×10^9 molecules of TNT can be sensed using a 1 mm fiber. Although the development in electrospinning techniques for fabricating nanofibers as sensors is quite substantial, a hybrid fiber with the dual properties of conductivity and luminescence has not been reported yet.

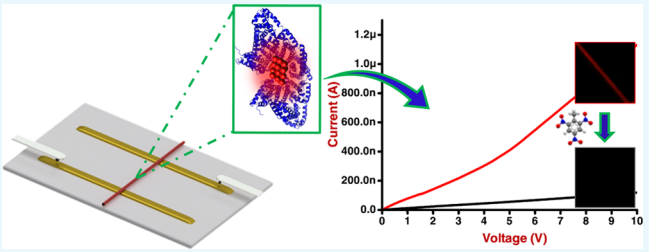

INTRODUCTION

Atomically precise clusters of noble metals encapsulated in proteins belong to an expanding area of research.[1] Because of their diverse properties they have been used in areas, such as catalysis,[2,3] energy,[4] sensors,[5] biomedicine,[6−8] and environment.[9] One of the most fascinating properties of such materials is luminescence, which has been used extensively in sensing,[5,10] mostly in solutions. On the basis of this inherent property, the protein-protected noble metal clusters were deemed to be a new class of nanoscale sensors for label-free detection of various biomolecules, such as protease[11] and hemoglobin[12] as well as several metal ions[13−15] and others. Sensing is mainly due to the large quantum yield and associated enhancement in emission upon binding on solid surfaces, enabling extremely low levels of detection down to a few tens of ions. Research on the use of these materials as optical sensors[10] using luminescence has been so intense that the possibility of utilizing the same clusters as conductivity sensors has not been considered seriously. The luminescence of protein-protected clusters (PPCs) arise from the intraband transitions in the cluster.[16] The existing literature suggests that proteins in both dry and wet states are capable of increasing the conductivity of a system as they are semiconducting in nature.[17] The protein protecting the cluster can also contribute to conductivity. Besides, free protein present along with PPCs also contribute to conductivity. During the formation of the metallic core, interprotein metal-ion transfer occurs in the solution, leading to the regeneration of free proteins from protein−metal adducts.[16] Increase in the core size within a protein further increases the free protein content in the solution.[18] To utilize both the conductivity and luminescence attributes of the protein-protected cluster to the maximum, suitable detection techniques and substrates are required.

Most of the detection protocols at the device level prefer electrical conductivity-based probes because of the ease of fabrication, cheaper components, and their quantitative analysis. Optical sensors have also started making an impact in the field of lab-on-a-chip devices owing to the miniaturization of the various components involved in it, providing faster on-the-spot qualitative analysis. A platform combining these two sensors provides quantitative and qualitative analysis, reducing false alarms. A dual mode sensor can be useful in point-of-use devices with extreme sensitivity. Incorporation of clusters in suitably modified electrospun nanofibers enables the fabrication of such dual mode sensors.

Electrospinning as a fabrication technique has acquired prominence in the area of sensors due to its versatility and flexibility. On the basis of the materials used, electrospun fibers can be used as conductivity sensors,[19−21] optical sensors,[22,23] strain sensors,[24,25] electrochemical sensors,[26] etc. Electrospinning is considered to be a versatile technique as it allows the user to play around with materials to modify the inherent ability of the polymer utilized. Composite fibers produced using electrospinning find applications in various areas.[27] Additionally, coaxial electrospinning provides the opportunity to make hybrid fibers out of two or more completely different materials,

Received: August 21, 2017
Accepted: October 11, 2017
Published: November 3, 2017

DOI: 10.1021/acsomega.7b01219
ACS Omega 2017, 2, 7576−7583

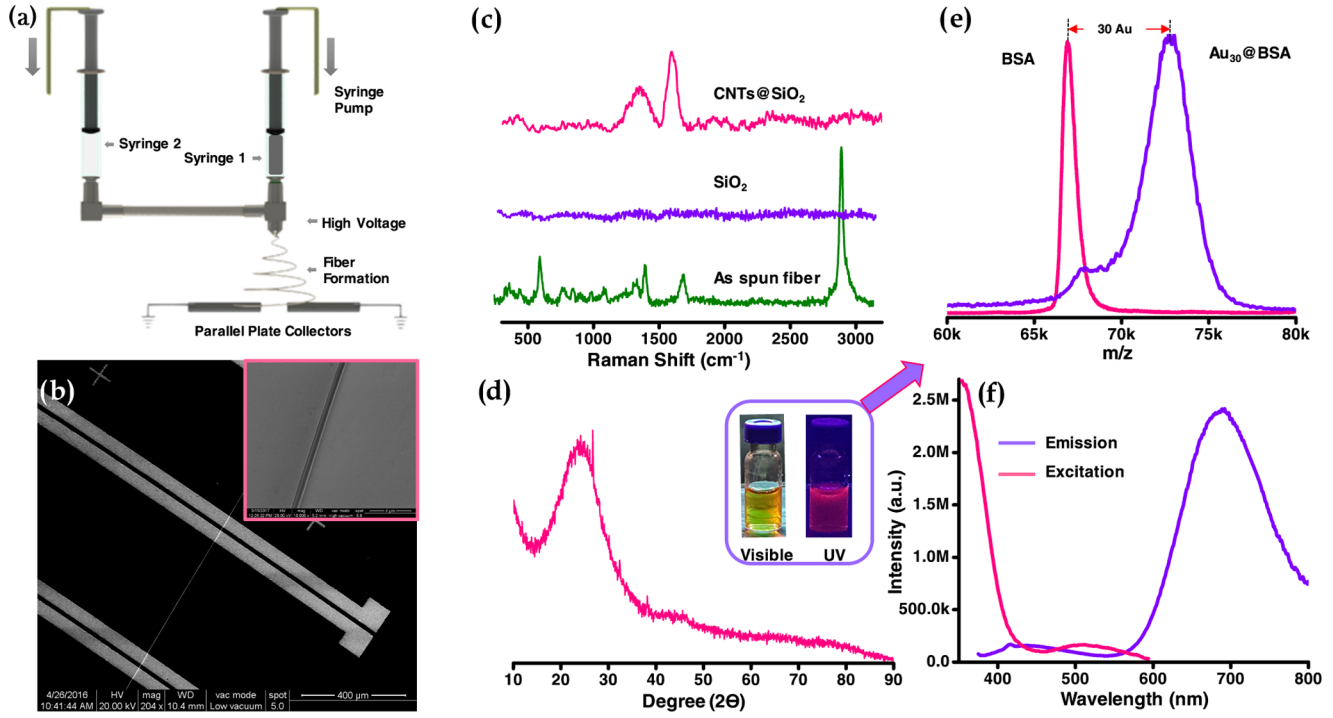

Figure 1. (a) Coaxial electrospinning setup; (b) scanning electron microscopy (SEM) image of a single fiber on the electrode assembly; inset shows a single fiber at higher magnification; (c) Raman spectra of the fibers (green trace: as-spun fiber before carbonization, violet trace: SiO_2 fibers post carbonization, pink trace: CNTs@SiO_2 fibers post carbonization); (d) X-ray diffraction (XRD) of the fibers, (inset shows the Au@BSA cluster under visible and UV light); (e) matrix-assisted laser desorption ionization mass spectra (MALDI-MS) of BSA and Au@BSA; and (f) excitation and emission spectra of the Au@BSA cluster.

with each material adding a different functionality to a single fiber, allowing the use of such a fiber for various applications.[28] Oxide-based nanofibers have carved a niche as gas sensors[29] either by conductivity[30,31] or by optical properties.[32] Conducting additives like carbon nanotubes (CNTs), graphene, etc., have been utilized to enhance the conductivity of a conducting polymer or to induce it in a usually insulating fiber.[27] Although the development of nanofibers as conductivity sensors or optical sensors is individually an extensively researched area, a fiber which can combine both these properties has not been fabricated to the best of our knowledge.

The main deterrent for the development of fibers with dual functionality of conductivity and luminescence is the common dark color of conducting polymers, which make them inappropriate as luminescent substrates. The main aspect of this article is to show that protein-protected clusters immobilized on a composite fiber with a conducting core and a dielectric shell can be utilized as dual functionality sensors. Thus, as a whole, the system acts like a lab-on-a-fiber. The amorphous nature of the dielectric material used helps to act as a good host for the cluster and can be conjugated with the cluster by either surface modification or simply by physisorption. In this article, we have utilized the multiwalled carbon nanotube (MWCNT) core with silica (SiO_2) sheath fibers obtained in a dual-step synthesis process for sensing. These fibers were then utilized to host Au@BSA clusters, which were further utilized to demonstrate the dual mode sensing strategy using an analyte of large social relevance. We have focused on the ability of bovine serum albumin (BSA) to conjugate with the nitro groups in trinitrotoluene for selective sensing.

RESULTS AND DISCUSSION

Structural and Morphological Characteristics. Unidirectionally aligned nanofibers were electrospun, as discussed before, with a parallel plate collector[12] modified for the use of coaxial spinneret, as shown in Figure 1a. The parallel plate alignment of the ground consists of two indium tin oxide (ITO) plates separated at a distance of 2.5 cm. This alignment of the ground facilitates the collection of a single nanofiber or multiple nanofibers as required. To deposit a single nanofiber on the substrate, electrospinning was done for 2 s at 25 kV. Because of the short time duration, very few fibers were deposited onto the ground. The fibers act as a bridge to connect the space between the parallel plates. These fibers are then lifted onto the substrate manually. These fibers are submerged in octane overnight to remove the mineral oil and then carbonized at 350 °C for 4 h. The fibers consisted of a CNT core and a porous SiO_2 shell. The core size of the SiO_2 layer is around 1−1.5 nm, as shown by transmission electron microscopy (TEM) measurements (Figure S-1).

The morphology of the as-prepared and carbonized nanofibers was analyzed using SEM, as shown in Figures S-2 and 1b, respectively. The inset of Figure 1b shows the fiber at a higher magnification. The as-prepared fibers were ∼900 nm in diameter, whereas the carbonized fibers were in the range of 600−700 nm. Shrinking of the fibers post carbonization by 150−200 nm is attributed to the loss of solvents and the polymer during heating. Raman spectra of the fibers at various stages were collected to understand the chemical composition of the fibers, as depicted in Figure 1c. The green trace is of the fibers before carbonization. The spectrum shows sharp peaks at 2950, 1740, and 640 cm^{-1}, which can be attributed to aliphatic C−H stretching, C═O stretching, and C═O deformation,

DOI: 10.1021/acsomega.7b01219
ACS Omega 2017, 2, 7576−7583

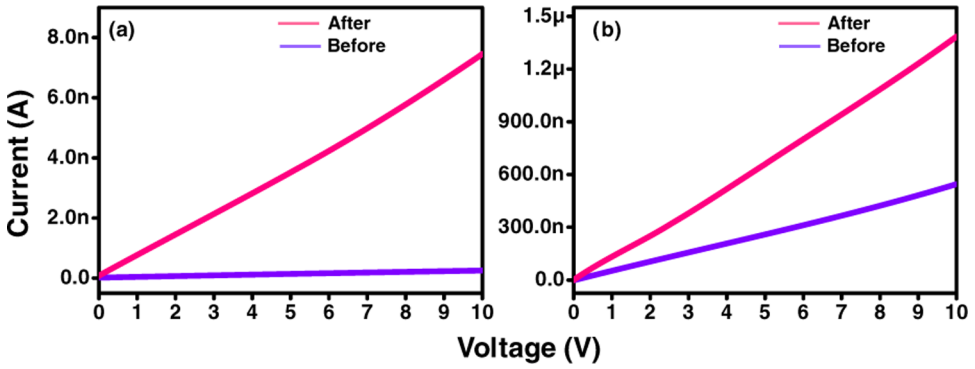

Figure 2. *I*−*V* characteristics of fibers before and after treatment with Au@BSA cluster. (a) SiO_2 fibers and (b) CNTs@SiO_2 fibers.

respectively. Multiple peaks in the range of 1450−1300 and 1200−1000 cm^{-1} arise due to C−H deformation and C−C stretching, respectively. The peaks between 600 and 300 cm^{-1} arise due to C−H in- and out-of-plane bending, and C−CH_2 out-of-plane bending.[33] The violet trace corresponds to only SiO_2 fibers that are electrospun without the CNTs and subsequently calcined at 350 °C. No characteristic Raman peaks were observed in the spectrum, which might be because of the amorphous nature of SiO_2 in the fiber. As the Raman is collected post calcination, the peaks arising from the polymer poly(vinyl acetate) (PVAc) are not present. The pink trace is of the carbonized CNTs@SiO_2 fiber mat. These show the characteristic D and G bands that correspond to the carbon nanotubes in the fiber. The XRD spectra in Figure 1d of the fibers show a prominent wide peak at 22° that corresponds to amorphous silica. As the concentration of CNTs is too low compared to that of SiO_2, no features of CNTs are visible. The photographs in the inset of Figure 1d correspond to the Au@BSA cluster in visible and UV light. The red luminescence of the cluster under UV light is stable. Figure 1e shows the MALDI-MS of the parent BSA protein and Au@BSA cluster. BSA shows a peak at 66.7 kDa, whereas the peak at around 72 kDa is attributed to the cluster indicating the formation of the Au_{30}@BSA cluster. Figure 1f shows the excitation and emission spectra of the cluster. The excitation peak at 320 nm and the emission peak at 630 nm also confirm the cluster formation. All of these data are in accordance with the previous reports.[18]

Electrical Characteristics. For characterizing the electrical properties of the nanofiber, substrates with single nanofibers were probed. To understand the difference in the current conduction before and after the cluster treatment, *I*−*V* studies of SiO_2 fibers and CNTs@SiO_2 fibers pre- and post-treatment were conducted and the data are plotted in Figure 2.

Figure 2a shows the *I*−*V* curve of silica fibers in the absence and presence of clusters. In the case of SiO_2 fibers, before the cluster treatment, the fibers do not show any current. Even though the fibers are SiO_2−carbon composites, the core is hollow and the carbon content in the shell as compared to silica is too low, which leads to high resistance, characteristic of amorphous silica. Coating the fiber with PPCs increases the current slightly, although still in the insulating regime. This slight increase can be attributed either to the proteins in the cluster which is on the surface and surrounding the fiber or the Na^+ ions present in the cluster solution. The absence of a conduction pathway hinders the movement of the charge carriers, leading to a low current.

In Figure 2b, the violet trace shows the *I*−*V* curve of CNTs@SiO_2 fiber. The fibers show current in the range of 500−600 nA at an applied voltage of 10 V. This proves that the core−shell fibers are conducting in nature. Fluctuations of the current in the above-mentioned range might be because of the variations in the loading of CNTs in each fiber. The presence of carbon in the outer shell of the fiber from the polymeric backbone and the pores in the silica are expected to provide a transduction pathway for electrons to flow to the CNTs in the core, thus providing a linear current. The pink trace corresponds to the *I*−*V* curve of the same fibers after they have been treated with Au@BSA and washed subsequently. An increase of more than two times is observed in the current of the functionalized fibers as compared to that of its precursor, with the current being in the range of 1.4 μA. The diameter of the protein-protected cluster is ∼5 nm; hence, the possibility of its penetration through the silica shell and direct interaction with the core is ruled out. The increase in current may be attributed to a combination of electron hopping from the cluster to the CNTs and the presence of free Na^+ ions on the surface of the fiber.

CNTs are well known to act as electron acceptors in a conducting system, whereas the PPCs can act as electron donors. The presence of carbon in the shell, although minimal, might play a role in providing a transduction pathway for electron transfer from the cluster to the core. The chemical pathway of the formation of protein-protected clusters has been studied and release of proteins during the synthesis process has been established.[16] The conduction of electricity by proteins is a known phenomenon although investigations are still underway to determine the exact factors responsible. Specifically, BSA has a semiconducting nature with activation energy of 2 eV,[34] which is close to the activation energy of CNTs.[35] Coating BSA on the fiber shows a high current, as shown in Figure S-3, although the current is not stable and decreases substantially in repetitive cycles. In contrast to this, the fibers coated with Au@BSA cluster exhibit a moderate current that is highly stable, as given in Figure S-4. A reasonable conjecture is to assume that the presence of gold cluster in the proteins decreases its activation energy while increasing the inherent conductivity and thus regulating the proton transfer, leading to the observation of a stable current. This conjecture is backed by a decrease in current of the system in presence of TNT as the nitro groups of TNT bind to the amino groups in BSA, decreasing the charge carriers in the system (explanation provided later). The other possibility for the increasing current might be the presence of Na^+ and Cl^- ions that are supplied from the cluster, although the literature suggests that even in the presence of such ions, the conductivity in proteins is predominantly due to mobile protons.[36] The stability of the

DOI: 10.1021/acsomega.7b01219
ACS Omega 2017, 2, 7576−7583

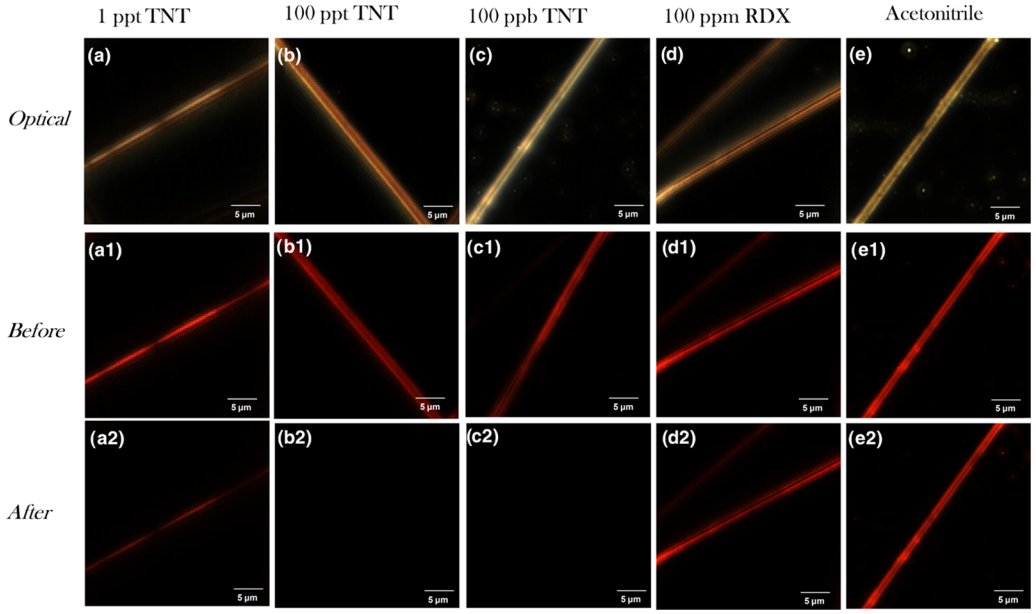

Figure 3. Optical and fluorescence images of the fibers in presence of various analytes.

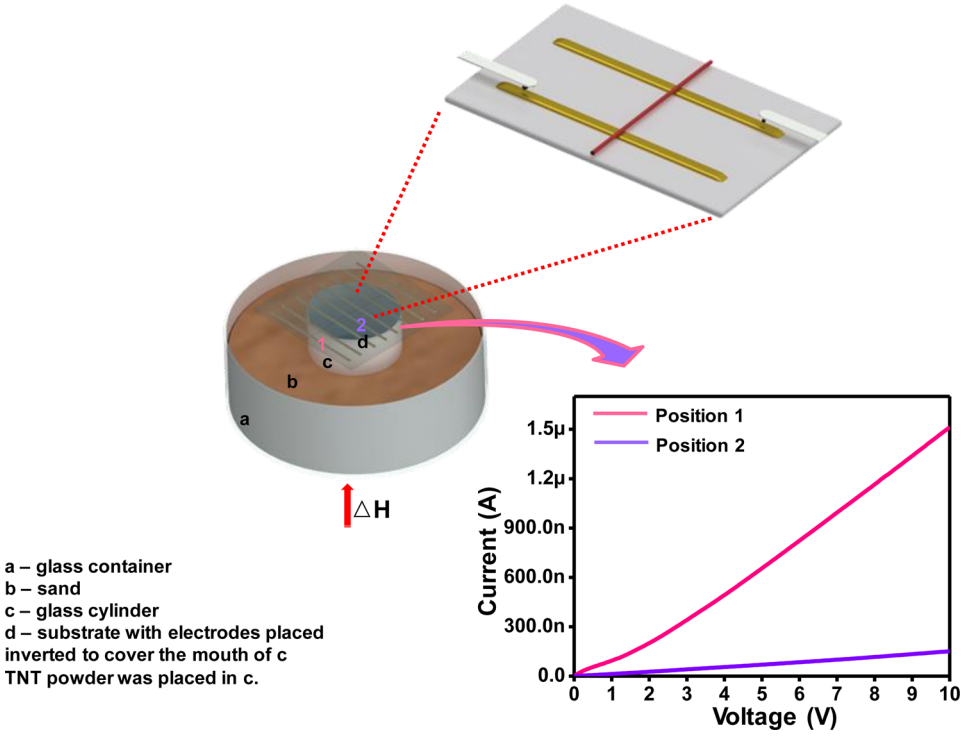

Figure 4. Schematic of setup for vapor-sensing experiments. Inset shows the fiber on the electrodes which is probed for $I-V$ studies and the current variation with exposure to TNT.

cluster-coated fiber has been checked up to 48 h, and no decrease in the $I-V$ characteristics was noted, as represented in Figure S-5.

Sensing Experiment. Sensitivity of Au@BSA clusters toward TNT has been explained by the formation of a Meisenheimer complex between the nitro group of the TNT and the free amino groups present in BSA.[37] This was also established by the change in the photoluminescence profile of the Au@BSA cluster after the addition of TNT, as shown in Figure S-6. Intense scattering from the silica fibers caused interference in the measurement of the photoluminescence spectrum of the composite. The physisorption of the cluster on the fiber enables them to detect TNT in both solution and the vapor phase. For the solution phase experiments, 2.5 μL of the analyte was introduced onto the luminescent fiber and luminescence quenching was analyzed using a fluorescence microscope. The dependence of the fiber sensitivity toward the concentration of TNT, acetonitrile, and its response to another commonly utilized explosive material is shown in Figure 3.

In Figure 3, images (a−e) correspond to the optical images of the cluster-coated fiber before the introduction of the analyte. The (a1−e1) images are the fluorescence images of the

DOI: 10.1021/acsomega.7b01219
ACS Omega 2017, 2, 7576−7583

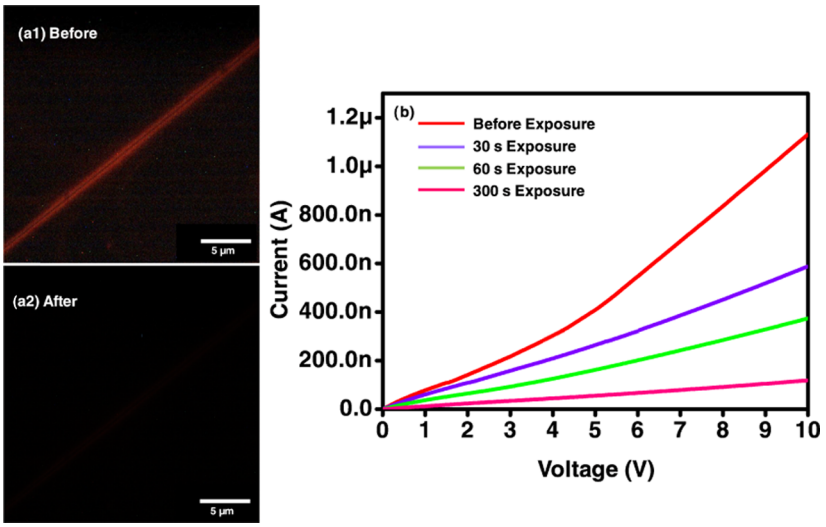

Figure 5. Exposure to TNT vapor: fluorescence measurements of the fibers (a1) before exposure, (a2) after 30 s exposure, (b) *I*−*V* measurements of the fibers with varying time.

fiber/fibers before the introduction of the analyte, whereas the (a2−e2) images are the fluorescence images taken a few seconds after the analyte has been introduced. Figure 3a2−c2 corresponds to the luminescence quenching of the fiber at varying concentrations of TNT, ranging from 1 ppt to 100 ppb. It can be seen that at 100 ppt and above, complete luminescence quenching is observed at 1 ppt, although not completely quenched, a noticeable level of decrease was noticed.

The number of TNT molecules required to bring about the quenching in Figure 3a2 is calculated to be 119, when the fiber length is taken to be 40 μm, as per the calculation shown in S-7. Figure 3d2 shows the fiber's response to 100 ppm of RDX. Although the concentration taken is very high as compared to TNT, the decrease in luminescence intensity is miniscule. As the TNT was dissolved in acetonitrile, to prove that the luminescence quenching was happening due to the TNT molecules and not due to solvent, a control experiment in which acetonitrile was introduced to the cluster-coated fibers is shown in Figure 3e2. No change in luminescence was observed proving that the solvent plays no role in the quenching mechanism.

For the vapor phase experiments, the setup consisted of the inverted substrate utilized as a lid for the container containing the analyte, kept in a sand bath. This was to ensure that the fibers are in direct contact with TNT vapor when an external temperature of 70 °C was applied, as shown in Figure 4. Another added advantage of the setup was that the same fiber being exposed to vapor was extended onto another set of electrodes on the substrate outside the exposure zone. Hence, the same fiber has both analyte-exposed and unexposed areas for which *I*−*V* studies can be done and variations in current at these positions were compared. The graph in Figure 4 shows the difference in the conductivity of the fiber at the exposed and unexposed zones with clear visible decrease in the current conduction where the fiber has come in contact with TNT.

Figure 5a1 shows the fluorescence image of the cluster-coated fiber. Figure 5a2 shows the fluorescence image of the same fiber, as shown in Figure 5a1, after exposure to TNT vapor for 30 s. Complete luminescence quenching is noted when the cluster-coated fibers are exposed to TNT vapor. Figure 5c shows the change in current of the fiber with varying exposure times (30−300 s) of TNT vapor. When exposed to the TNT vapor, within 30 s, the inherent current of the fiber decreases to about half of the initial value and with increasing exposure time, the conductivity of the fiber was lost and it reached the insulator regime. The exposure measurements were done taking the fiber length as 1 mm, on the basis of the channel width and because the approximate diameter of the fiber was known from SEM measurements, the area of exposure could be calculated.

Assuming that the cluster forms a monolayer covering on the fiber, the number of TNT molecules required for Meisenheimer complexation to occur between TNT and BSA in the exposed region is about 10^9, whereas the number of TNT molecules present in the container at a temperature of 70 °C is about 10^{12}. Thus, adequate molecules are present for the reaction to happen. Detailed calculations are given in S-8. The number of molecules required for sensing to happen can be further decreased by modifying the interelectrode distance. The decrease in the fiber current intensity does not happen instantaneously but with increase in the exposure time, which might be attributed to the excess cluster present on the fiber surface. The nanoporous surface of the fiber facilitates the diffusion of the vapors[38] inside the fiber, allowing Meisenheimer complex formation to occur, leading to high sensitivity. Although there is a significant decrease in the current after TNT exposure, exposing the fiber to air afterward for a few hours allows the fiber to regain the conductivity to that before the cluster treatment, as can be seen in Figure S-9. The specificity of the fiber was analyzed by comparing it with the closest analogue of TNT, namely 2,4-dinitrotoluene (DNT). Fluorescence imaging shows the change in the fluorescence of the fibers after exposing the fibers to DNT vapors for 30 s. The quenching is substantial although a trace level of cluster luminescence can still be observed while using conductance measurements; current decrease in the fiber when exposed to DNT was approximately 50% after 5 min (Figure S-10) compared with the same depletion within 30 s in presence of TNT.

Meisenheimer complex formation happens between the electron withdrawing groups and nucleophiles, i.e., electron

DOI: 10.1021/acsomega.7b01219
ACS Omega 2017, 2, 7576−7583

donating groups. The increase in electrical conductivity of cluster-coated fibers is attributed to the conducting nature of the proteins, mostly aromatic amino acids. Exposure of the fiber to TNT brings about the interaction of amino acids with the nitro groups. Nitro groups being electron withdrawing groups form adducts with the amino acids, leading to a decrease in the charge carriers of the fiber, leading to an overall decrease in the electrical conductivity of the fiber. A schematic representing the formation of the Meisenheimer complex in our system is given in Figure S-11.

CONCLUSIONS

In the present article, we introduce the functional ability of protein-protected clusters to act as conductivity sensors along with them being utilized as luminescence sensors. Hosting these clusters on dielectric porous shell nanofibers with conducting cores allows qualitative and quantitative measurements to be done with high precision, both in solution and in the vapor phase. In the solution phase, TNT can be detected down to 1 ppt at room temperature, whereas in the vapor phase, 4.8×10^9 molecules of TNT can be sensed using a 1 mm fiber. The cluster-immobilized fibers show high sensitivity and specificity to TNT in vapor phase; when further developed these can be used as disposable sensors for TNT in point-of-use devices.

EXPERIMENTAL SECTION

Materials and Methods. Poly(vinyl acetate) (PVAc) (MW 10 000 Da) was purchased from Alfa Aesar. Ethanol, propane-2-ol, acetone, and hydrochloric acid (HCl) were purchased from Fisher Scientific. Mineral oil (liquid paraffin) and octane were obtained from Spectrochem. Tetraethoxysilane (TEOS), MWCNTs of average length of 110 nm, and 2,4-dinitrotoluene (DNT) were purchased from Sigma-Aldrich. Sodium hydroxide (NaOH) was purchased from Rankem, India. Bovine serum albumin (BSA) was purchased from Sisco Research Laboratories. 2,4,6-Trinitrotoluene (TNT) and hexahydro-1,3,5-trinitro-1,3,5-triazine (RDX) were gifts from Indira Gandhi Centre for Atomic Research, Kalpakkam, India. All chemicals were of analytical grade and were used without further purification. Triply distilled water was used throughout the experiments.

Synthesis of Au@BSA Cluster. The Au@BSA nanoclusters with red luminescence were prepared following a reported method[18] by adding aqueous solution of $HAuCl_4$ (10 mL, 6 mM) to BSA (10 mL, 25 mg/mL in water) under vigorous stirring for 5 min. The pH of the solution was adjusted to around 11.0 with the addition of NaOH (1 mL, 1 M). The reactions were kept for 24 h. The solution turned from pale yellow to dark orange, with deep red emission, indicating the formation of Au@BSA nanoclusters. The sample was stored at 4 °C.

Instrumentation. Electrospinning was done by utilizing an ESPIN-NANO needle-based electrospinning machine. UV−vis spectra were recorded using a PerkinElmer Lambda 25 spectrophotometer. Scanning electron microscopy (SEM) images and energy-dispersive analysis of X-ray (EDAX) studies were performed using a FEI QUANTA-200 SEM. Raman measurements were done with a WiTec GmbH, CRM RS300 instrument having a 532 nm Nd:YAG laser as the excitation source, and the dispersed light intensity was measured by a Peltier-cooled charge coupled device. The photoexcitation and luminescence (PL) studies were done using a NanoLog HORIBA JOBINYVON spectrofluorimeter. Fluorescence imaging measurements were done with the Cytoviva HSI system containing an Olympus BX-41 microscope equipped with a Dage high resolution camera and a Specim V10E spectrometer. Dark field fluorescence microscopy was used with an excitation band at 492 ± 18 nm, and emission was collected using a triple pass emission filter DAPI/FITC/TEXAS RED (DAPI, 452−472 nm; FITC, 515−545 nm; TEXAS RED, 600−652 nm). The electrical measurements were done using Cascade Microtek Summit 11000 M probe station.

Preparation of SiO_2 and MWCNTs@SiO_2 Fibers. For the preparation of SiO_2 fibers, a reported method[39] was followed utilizing coaxial electrospinning. For the shell solution, TEOS (3.66 mL) was hydrolyzed by adding ethanol (3.26 mL) to TEOS under vigorous stirring for 1 h. To the solution, HCl (0.06 mL) was added and stirred for 1 h. Subsequently deionized water (1.81 mL) was added to the solution and left for stirring overnight. To this solution, PVAc (1.75 g) was added and stirred further for 4 h.

The above-mentioned solution was taken in the outer syringe and mineral oil was taken in the inner syringe of the coaxial setup. MWCNTs@SiO_2 fibers were obtained by the addition of MWCNTs to the mineral oil in the inner syringe of the coaxial spinneret. MWCNTs will be referred to as CNTs throughout the text. The coaxial spinneret consists of the core needle size of 18 G. The shell solution was fed at a rate of 1.2 mL/h and that of the core at 0.6 mL/h, with an applied voltage of 25 kV. The tip-to-collector distance was set to 10 cm. The as-spun fibers were collected on parallel indium tin oxide (ITO) plates separated by 2.5 cm gap and manually transferred to electrodes patterned on glass or silicon wafer and immersed in octane for 12 h to remove mineral oil existing in the core of the as-spun fibers. The fibers were dried and subsequently carbonized at 350 °C for 4 h to remove remaining mineral oil (ignition temperature ∼230 °C) solvents and to carbonize the polymer present.

Preparation of SiO_2@Au@BSA and CNTs@SiO_2@Au@BSA Fibers. For the preparation of Au@BSA-coated SiO_2 fibers, the cluster solution was drop cast on the substrate containing the fibers and left for 15 min. The substrates were then washed with water and dried at room temperature for 3 h and used. The same protocol was followed to obtain CNTs@SiO_2@Au@BSA fibers.

Electrode Fabrication. The gold electrodes on the silicon wafer were patterned using photolithography, which was preceded by washing of the silicon substrate in hot acetone, followed by boiling isopropanol (IPA) and then rinsed with deionized (DI) water. Electrodes were obtained using a lift-off process. The wafer was then blow dried and stored in vacuum for further use. The gold electrodes were 100 μm wide, with a thickness of 120 nm. The interelectrode distance was 20 μm. These electrodes were utilized mostly for SEM measurements.

For most of the experimental purposes, ITO electrodes on glass substrates, henceforth referred to as the substrates, were utilized, as transparency of glass was crucial for fluorescence experiments. For the fabrication of these electrodes, an ITO-coated glass slide was cleaned by blowing air and then patterned using lithography. ITO was etched using dilute HCl for about 10 min. The substrate was then washed in boiling acetone, then IPA, followed by rinsing in DI water and dried by blowing air and finally stored in vacuum till required. The electrodes were of 300 μm width and 150 nm height. The

DOI: 10.1021/acsomega.7b01219
ACS Omega 2017, 2, 7576−7583

distance between the two electrodes was 1 mm that acted as the channel.

Fluorescence Sensing Experiment. For the single fiber sensing experiment, we placed the cluster-coated fiber under the microscope. About 2.5 μL of the analyte solution was added on the fiber. Fluorescence images of the fiber were taken before and after addition of the analyte.

Conductance Sensing Experiment. For the conductance measurements, the fiber was placed in a probe station. The probes utilized are gold-coated tungsten, with a tip diameter of 20 μm.

Vapor-Based Experiments. The fiber-containing substrate was placed at the mouth of the beaker in which the analyte was placed. The beaker was subsequently heated to 70 °C by placing it in a sand bath. The substrate was then removed as required and kept in a sealed environment to minimize air exposure. A detailed explanation of the setup with a schematic is provided in Results and Discussion.

■ ASSOCIATED CONTENT

Supporting Information

The Supporting Information is available free of charge on the ACS Publications website at DOI: 10.1021/acsomega.7b01219.

TEM and SEM characterizations of the fibers, *I*−*V* studies of the fibers, calculations for the fluorescence and vapor experiments, and study regarding exposure to DNT (PDF)

■ AUTHOR INFORMATION

Corresponding Author

*E-mail: pradeep@iitm.ac.in.

ORCID

Thalappil Pradeep: 0000-0003-3174-534X

Notes

The authors declare no competing financial interest.

■ ACKNOWLEDGMENTS

We are thankful to the Department of Science and Technology, India, for constantly supporting our research on nanomaterials. The authors are thankful to the Centre for NEMS and Nanophotonics (CNNP), IIT Madras for facilitating the device fabrication and electrical measurements. V.S. is thankful to IIT Madras for the student fellowship.

■ REFERENCES

(1) Lu, Y.; Chen, W. Sub-nanometre sized metal clusters: from synthetic challenges to the unique property discoveries. *Chem. Soc. Rev.* **2012**, *41*, 3594−3623.

(2) Yamazoe, S.; Koyasu, K.; Tsukuda, T. Nonscalable Oxidation Catalysis of Gold Clusters. *Acc. Chem. Res.* **2014**, *47*, 816−824.

(3) Liu, Y.; Zheng, Y.; Du, B.; Nasaruddin, R. R.; Chen, T.; Xie, J. Golden Carbon Nanotube Membrane for Continuous Flow Catalysis. *Ind. Eng. Chem. Res.* **2017**, *56*, 2999−3007.

(4) Mathew, A.; Pradeep, T. Noble Metal Clusters: Applications in Energy, Environment, and Biology. *Part. Part. Syst. Charact.* **2014**, *31*, 1017−1053.

(5) Ghosh, A.; Jeseentharani, V.; Ganayee, M. A.; Hemalatha, R. G.; Chaudhari, K.; Vijayan, C.; Pradeep, T. Approaching Sensitivity of Tens of Ions Using Atomically Precise Cluster−Nanofiber Composites. *Anal. Chem.* **2014**, *86*, 10996−11001.

(6) Zheng, K.; Setyawati, M. I.; Leong, D. T.; Xie, J. Antimicrobial Gold Nanoclusters. *ACS Nano* **2017**, *11*, 6904−6910.

(7) Goswami, N.; Luo, Z.; Yuan, X.; Leong, D. T.; Xie, J. Engineering gold-based radiosensitizers for cancer radiotherapy. *Mater. Horiz.* **2017**, *4*, 817−831.

(8) Govindaraju, S.; Ankireddy, S. R.; Viswanath, B.; Kim, J.; Yun, K. Fluorescent Gold Nanoclusters for Selective Detection of Dopamine in Cerebrospinal fluid. *Sci. Rep.* **2017**, *7*, No. 40298.

(9) Jin, R.; Zeng, C.; Zhou, M.; Chen, Y. Atomically Precise Colloidal Metal Nanoclusters and Nanoparticles: Fundamentals and Opportunities. *Chem. Rev.* **2016**, *116*, 10346−10413.

(10) Chen, L.-Y.; Wang, C.-W.; Yuan, Z.; Chang, H.-T. Fluorescent Gold Nanoclusters: Recent Advances in Sensing and Imaging. *Anal. Chem.* **2015**, *87*, 216−229.

(11) Madadrang, C. J.; Kim, H. Y.; Gao, G.; Wang, N.; Zhu, J.; Feng, H.; Gorring, M.; Kasner, M. L.; Hou, S. Adsorption Behavior of EDTA-Graphene Oxide for Pb (II) Removal. *ACS Appl. Mater. Interfaces* **2012**, *4*, 1186−1193.

(12) Yang, D.; Meng, H.; Tu, Y.; Yan, J. A nanocluster-based fluorescent sensor for sensitive hemoglobin detection. *Talanta* **2017**, *170*, 233−237.

(13) Yue, Y.; Liu, T.-Y.; Li, H.-W.; Liu, Z.; Wu, Y. Microwave-assisted synthesis of BSA-protected small gold nanoclusters and their fluorescence-enhanced sensing of silver(i) ions. *Nanoscale* **2012**, *4*, 2251−2254.

(14) Durgadas, C. V.; Sharma, C. P.; Sreenivasan, K. Fluorescent gold clusters as nanosensors for copper ions in live cells. *Analyst* **2011**, *136*, 933−940.

(15) He, J.; Liu, M.; Gao, F.; Gao, L.; Gao, X.; Han, R. Biomimetic construction of protein-conjugated gold clusters for detecting Hg2+. *Colloids Surf., A* **2017**, *518*, 80−84.

(16) Chaudhari, K.; Xavier, P. L.; Pradeep, T. Understanding the Evolution of Luminescent Gold Quantum Clusters in Protein Templates. *ACS Nano* **2011**, *5*, 8816−8827.

(17) Rosenberg, B. Electrical Conductivity of Proteins. *Nature* **1962**, *193*, 364−365.

(18) Mohanty, J. S.; Baksi, A.; Lee, H.; Pradeep, T. Noble metal clusters protected with mixed proteins exhibit intense photoluminescence. *RSC Adv.* **2015**, *5*, 48039−48045.

(19) Andre, R. S.; Shimizu, F. M.; Miyazaki, C. M.; Riul, A., Jr.; Manzani, D.; Ribeiro, S. J. L.; Oliveira, O. N., Jr.; Mattoso, L. H. C.; Correa, D. S. Hybrid layer-by-layer (LbL) films of polyaniline, graphene oxide and zinc oxide to detect ammonia. *Sens. Actuators, B* **2017**, *238*, 795−801.

(20) Li, C.; Chartuprayoon, N.; Bosze, W.; Low, K.; Lee, K. H.; Nam, J.; Myung, N. V. Electrospun Polyaniline/Poly(ethylene oxide) Composite Nanofibers Based Gas Sensor. *Electroanalysis* **2014**, *26*, 711−722.

(21) Zhang, Y.; Kim, J. J.; Chen, D.; Tuller, H. L.; Rutledge, G. C. Electrospun Polyaniline Fibers as Highly Sensitive Room Temperature Chemiresistive Sensors for Ammonia and Nitrogen Dioxide Gases. *Adv. Funct. Mater.* **2014**, *24*, 4005−4014.

(22) Shehata, N.; Samir, E.; Gaballah, S.; Hamed, A.; Elrasheedy, A. Embedded Ceria Nanoparticles in Crosslinked PVA Electrospun Nanofibers as Optical Sensors for Radicals. *Sensors* **2016**, *16*, 1371.

(23) Camposeo, A.; Moffa, M.; Persano, L. Electrospun Fluorescent Nanofibers and Their Application in Optical Sensing. In *Electrospinning for High Performance Sensors*; Macagnano, A.; Zampetti, E.; Kny, E., Eds.; Springer International Publishing: Cham, 2015; Vol. 129−155.

(24) Yu, G.-F.; Li, J.-T.; Pan, W.; He, X.-X.; Zhang, Y.-J.; Gong, M.-G.; Yu, M.; Zhang, Z.-M.; Long, Y.-Z. Electromagnetic functionalized ultrafine polymer/γ-Fe2O3 fibers prepared by magnetic-mechanical spinning and their application as strain sensors with ultrahigh stretchability. *Compos. Sci. Technol.* **2017**, *139*, 1−7.

(25) Jia, X.-S.; Tang, C.-C.; Yan, X.; Yu, G.-F.; Li, J.-T.; Zhang, H.-D.; Li, J.-J.; Gu, C.-Z.; Long, Y.-Z. Flexible Polyaniline/Poly(methyl methacrylate) Composite Fibers via Electrospinning and In Situ Polymerization for Ammonia Gas Sensing and Strain Sensing. *J. Nanomater.* **2016**, 1−8.

DOI: 10.1021/acsomega.7b01219
ACS Omega 2017, 2, 7576−7583

(26) Mondal, K.; Sharma, A. Recent advances in electrospun metal-oxide nanofiber based interfaces for electrochemical biosensing. *RSC Adv.* **2016**, *6*, 94595−94616.
(27) Abideen, Z. U.; Park, J. Y.; Kim, H. W.; Kim, S. S. Graphene-loaded tin oxide nanofibers: optimization and sensing performance. *Nanotechnology* **2017**, *28*, No. 035501.
(28) Qu, H.; Wei, S.; Guo, Z. Coaxial electrospun nanostructures and their applications. *J. Mater. Chem. A* **2013**, *1*, 11513−11528.
(29) Wetchakun, K.; Samerjai, T.; Tamaekong, N.; Liewhiran, C.; Siriwong, C.; Kruefu, V.; Wisitsoraat, A.; Tuantranont, A.; Phanichphant, S. Semiconducting metal oxides as sensors for environmentally hazardous gases. *Sens. Actuators, B* **2011**, *160*, 580−591.
(30) Nguyen, T.-A.; Park, S.; Kim, J. B.; Kim, T. K.; Seong, G. H.; Choo, J.; Kim, Y. S. Polycrystalline tungsten oxide nanofibers for gas-sensing applications. *Sens. Actuators, B* **2011**, *160*, 549−554.
(31) Haiyan, L.; Xiang, W.; Guangqi, H.; Yihong, L.; Jin, W.; Jianyi, Z.; Gaofeng, Z.; Daoheng, S. In *Electrospun Nickel Oxide Nanofibers for Gas Sensor Application*, The 8th Annual IEEE International Conference on Nano/Micro Engineered and Molecular Systems, April 7−10, 2013; pp 377−380.
(32) Wang, P.; Wang, Y.; Tong, L. Functionalized polymer nanofibers: a versatile platform for manipulating light at the nanoscale. *Light: Sci. Appl.* **2013**, *2*, No. e102.
(33) Sanoria, A.; Ulbricht, D.; Schuster, T.; Brull, R. Monitoring crosslinking inhomogeneities in ethylene vinyl acetate photovoltaic encapsulants using Raman microscopy. *RSC Adv.* **2015**, *5*, 93522−93529.
(34) Rosenberg, B. Electrical Conductivity of Proteins. II. Semiconduction in Crystalline Bovine Hemoglobin. *J. Chem. Phys.* **1962**, *36*, 816−823.
(35) Bronikowski, M. J. Longer Nanotubes at Lower Temperatures: The Influence of Effective Activation Energies on Carbon Nanotube Growth by Thermal Chemical Vapor Deposition. *J. Phys. Chem. C* **2007**, *111*, 17705−17712.
(36) Bone, S.; Eden, J.; Pethig, R. Electrical properties of proteins as a function of hydration and NaCl content. *Int. J. Quantum Chem.* **1981**, *20*, 307−316.
(37) Mathew, A.; Sajanlal, P. R.; Pradeep, T. Inside Back Cover: Selective Visual Detection of TNT at the Sub-Zeptomole Level (Angew. Chem. Int. Ed. 38/2012). *Angew. Chem., Int. Ed.* **2012**, *51*, 9699.
(38) Che, Y.; Gross, D. E.; Huang, H.; Yang, D.; Yang, X.; Discekici, E.; Xue, Z.; Zhao, H.; Moore, J. S.; Zang, L. Diffusion-Controlled Detection of Trinitrotoluene: Interior Nanoporous Structure and Low Highest Occupied Molecular Orbital Level of Building Blocks Enhance Selectivity and Sensitivity. *J. Am. Chem. Soc.* **2012**, *134*, 4978−4982.
(39) Katoch, A.; Kim, S. S. Synthesis of Hollow Silica Fibers with Porous Walls by Coaxial Electrospinning Method. *J. Am. Ceram. Soc.* **2012**, *95*, 553−556.

DOI: 10.1021/acsomega.7b01219
ACS Omega 2017, 2, 7576−7583